



Effect of Annealing on the Magnetic Properties of FeCoNiCuNbSiB Soft Magnetic Alloys

Z. Li^{1*}, K. F. Yao^{2*}, T. C. Liu³, X. Li¹ and S. Wang¹

¹Institute of High Energy Physics, Chinese Academy of Science, Beijing, China, ²School of Material Science and Engineering, Tsinghua University, Beijing, China, ³China Iron and Steel Research Institute Group, Advanced Technology and Materials Co., Ltd., Beijing, China

A series of nanocrystalline soft magnetic alloys with nominal compositions of $\text{Fe}_{66.8-x}\text{Co}_{10}\text{Ni}_x\text{Cu}_{0.8}\text{Nb}_{2.9}\text{Si}_{11.5}\text{B}_8$ ($x = 1-15$ at%) were developed and studied. Effects of annealing on the soft magnetic properties, crystallization behavior, and domain structure were investigated. The alloys with higher Ni content were prone to exhibit stronger magnetic anisotropy. The $\text{Fe}_{66.8}\text{Co}_{10}\text{Ni}_{10}\text{Cu}_{0.8}\text{Nb}_{2.9}\text{Si}_{11.5}\text{B}_8$ alloy exhibited excellent soft magnetic properties, including the low permeability of 2000, low coercivity of about 0.6 A/m, and low remanence of 2.4 mT, together with a temperature gap of 128 K between two crystallization onset temperatures. It has been found that the Ni content and the annealing process possess significant effects on the soft magnetic property of the nanocrystalline alloys. It shows that the developed $\text{Fe}_{66.8}\text{Co}_{10}\text{Ni}_{10}\text{Cu}_{0.8}\text{Nb}_{2.9}\text{Si}_{11.5}\text{B}_8$ nanocrystalline alloy exhibits great potentials for applying in the field of common mode chokes or current transformers, due to its ability to resist the direct current.

Keywords: nanocrystallization, annealing, microstructure, soft magnetic properties, magnetic domain

OPEN ACCESS

Edited by:

Jiang Ma,
Shenzhen University, China

Reviewed by:

Ran Li,
Beihang University, China
Baoan Sun,
Institute of Physics (CAS), China

*Correspondence:

Z. Li
lz_kevin@163.com
K. F. Yao
kyao@tsinghua.edu.cn

Specialty section:

This article was submitted to
Ceramics and Glass,
a section of the journal
Frontiers in Materials

Received: 30 October 2021

Accepted: 19 November 2021

Published: 05 January 2022

Citation:

Li Z, Yao KF, Liu TC, Li X and Wang S
(2022) Effect of Annealing on the
Magnetic Properties of
FeCoNiCuNbSiB Soft Magnetic Alloys.
Front. Mater. 8:805609.
doi: 10.3389/fmats.2021.805609

INTRODUCTION

FINEMET-type FeCuNbSiB nanocrystalline alloys exhibit excellent comprehensive soft magnetic properties including high saturation magnetic induction B_s , high permeability μ , and low core loss P (Yoshizawa et al., 1988a). Furthermore, since FINEMET-type FeCuNbSiB nanocrystalline alloys can be easily prepared in air at low cost, they are widely used in electronic fields such as high-frequency power transformers, common mode chokes, magnetic amplifiers, and current transformers (Yoshizawa et al., 1988b; Petzold, 2002; Hasegawa, 2004; Herzer et al., 2005; Hasegawa, 2006; Herzer, 2013). Nowadays, the devices used in electronic and information fields, however, are prone to higher power and higher frequency. Then, it is necessary to develop soft magnetic materials with better permeability properties in high-frequency range and good DC resistance ability.

It is known that the performance of permeability vs. frequency in high-frequency regions could be enhanced by a large anisotropy constant K_u when the coercivity property does not deteriorate. This results in the decreases in permeability attenuation with frequency. This characteristic makes the design of the LCR rectifier circuit become easier when the material is processed into an inductor. The anisotropy constant K_u could be evaluated by Herzer et al. (2011)

$$K_u = \frac{H_k J_s}{2} \quad (1)$$

where H_k is the magnetic anisotropy field and J_s is the saturation magnetic polarization. As indicated by Eq. 1, the magnetic anisotropy constant K_u can be improved by increasing J_s . Nevertheless, despite there being myriad works focusing on developing materials with high saturation magnetic polarization (Makino et al., 1995; Ohta and Yoshizawa, 2007; Makino et al., 2009; Kubota et al., 2011; Urata et al., 2011; Chen et al., 2013; Li et al., 2014; Li et al., 2015; Shi and Yao, 2020; Shi et al., 2021), few of these materials can meet the requirements of industrial mass production. Moreover, the increase in magnetic anisotropy constant K_u is very limited.

For FINEMET-type alloys, the magnetic field-induced anisotropy is very weak (Herzer, 1994a). However, it was found that the creep could induce the anisotropy in FINEMET-type alloys (Herzer, 1994b). It shows a K_u value as large as $1,000 \text{ J/m}^3$ can be achieved after the FINEMET-type alloys are annealed with a 100-MPa tensile stress applied along the ribbon axis. However, due to the low productivity, inducing anisotropy *via* creep is impractical for industrial production.

For nanocrystalline alloys processed by magnetic field annealing, adding other ferromagnetic elements such as Co and Ni is considered to be conducive to the induction of in-plane anisotropy (Fujimori et al., 1977; Ohnuma et al., 2003; Yoshizawa et al., 2003). However, the crystallization process would be significantly influenced after the addition/replacement of Co and Ni to Fe-based amorphous alloys (Agudo and Vázquez, 2005). The increment of the Ni content leads to the rise of the second crystallization peak temperature of the amorphous alloy rise, resulting in the deterioration of the thermal stability and soft magnetic property of the alloy. Then, understanding the factors affecting the crystallization behavior and soft magnetic property of the nanocrystalline alloy is important.

Here, effects of Ni addition and annealing process on the structure and properties of FeCoNiCuNbSiB soft magnetic alloys were investigated, and an $\text{Fe}_{66.8}\text{Co}_{10}\text{Ni}_{10}\text{Cu}_{0.8}\text{Nb}_{2.9}\text{Si}_{11.5}\text{B}_8$ nanocrystalline alloy with good soft magnetic property and large resistance to direct current in the high-frequency region was obtained.

EXPERIMENTAL PROCEDURE

Alloy ingots with a nominal composition of $\text{Fe}_{66.8-x}\text{Co}_{10}\text{Ni}_x\text{Cu}_{0.8}\text{Nb}_{2.9}\text{Si}_{11.5}\text{B}_8$ ($x = 1, 5, 10, 15 \text{ at\%}$) were prepared by induction melting in a high-vacuum condition. The raw materials were industrial-purity metals of Fe (99.9 mass%), Co (99.9 mass%), Ni (99.9 mass%), Cu (99.9 mass%), Si (99.9 mass%), pre-alloyed Nb-Fe (99.7 mass%), and Fe-B (99.7 mass%). The amorphous ribbons were manufactured by the single-roll rapid solidification method. The ribbon width is 30 mm, and thickness is $22 \mu\text{m}$. The ribbons were slit to 6 mm in width. Toroidal cores with the outer diameter of 29 mm and inner diameter of 21 mm were wound by these slit ribbons then. These cores were annealed at different temperatures in a furnace with 2 L/min flowing argon; meanwhile, a 400-Oe transverse magnetic field

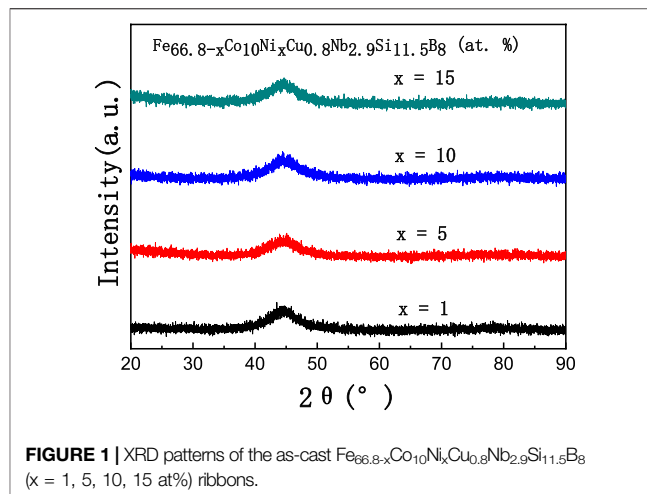


FIGURE 1 | XRD patterns of the as-cast $\text{Fe}_{66.8-x}\text{Co}_{10}\text{Ni}_x\text{Cu}_{0.8}\text{Nb}_{2.9}\text{Si}_{11.5}\text{B}_8$ ($x = 1, 5, 10, 15 \text{ at\%}$) ribbons.

was applied. The transverse field means the direction is parallel to the axis of rotation.

The microstructure of as-cast and annealed ribbons was analyzed by X-ray diffractometry (XRD, Bruker D8 Advance) with Cu K radiation ($\lambda = 0.15406 \text{ nm}$). The thermodynamic characteristics of the ribbons were analyzed by the differential scanning calorimeter (DSC, NETZSCH 404C) at a heating rate of 10 K/min under high-purity argon flow. The B-H loops were measured by a static magnetic property analyzer (MATS-2010SD). The core loss property of the cores was analyzed by the IWATSU B-H Analyzer. The test frequency range was $10\text{--}100 \text{ kHz}$, sinusoidal type. The maximum flux density values were 100, 200, and 300 mT, respectively. Images of the magnetic domain structures for samples with different compositions were captured using the magneto-optical Kerr microscope (Zeiss A $\times 10$). All measurements were performed at room temperature.

RESULTS AND DISCUSSION

The XRD patterns of the as-cast $\text{Fe}_{66.8-x}\text{Co}_{10}\text{Ni}_x\text{Cu}_{0.8}\text{Nb}_{2.9}\text{Si}_{11.5}\text{B}_8$ ($x = 1, 5, 10, 15 \text{ at\%}$) ribbons are shown in Figure 1. Except for the broad peak corresponding to the amorphous phase, no crystallization peak can be found in the XRD patterns, indicating that the microstructure of the as-cast ribbons is amorphous.

The DSC curves of the as-cast $\text{Fe}_{66.8-x}\text{Co}_{10}\text{Ni}_x\text{Cu}_{0.8}\text{Nb}_{2.9}\text{Si}_{11.5}\text{B}_8$ ($x = 1, 5, 10, 15 \text{ at\%}$) ribbons are shown in Figure 2. The first and second crystallization onset temperature T_{x1} and T_{x2} and the first and second crystallization peak temperature T_1 and T_2 are indicated by arrows on the curves. We can find three distinguishing characteristics in the DSC curves. Firstly, T_2 decreases gradually with the increase in Ni content, while T_1 stays almost unchanged. The temperature gap ΔT_x ($T_{x2} - T_{x1}$) shrinks down from 165 to 119 K with the increase in Ni content. However, the interval ΔT_x for the alloys with $x = 5, 10, 15$ are almost the same. This value agrees to the previous work by Agudo in Ref. (Agudo and Vázquez, 2005). Secondly, there is

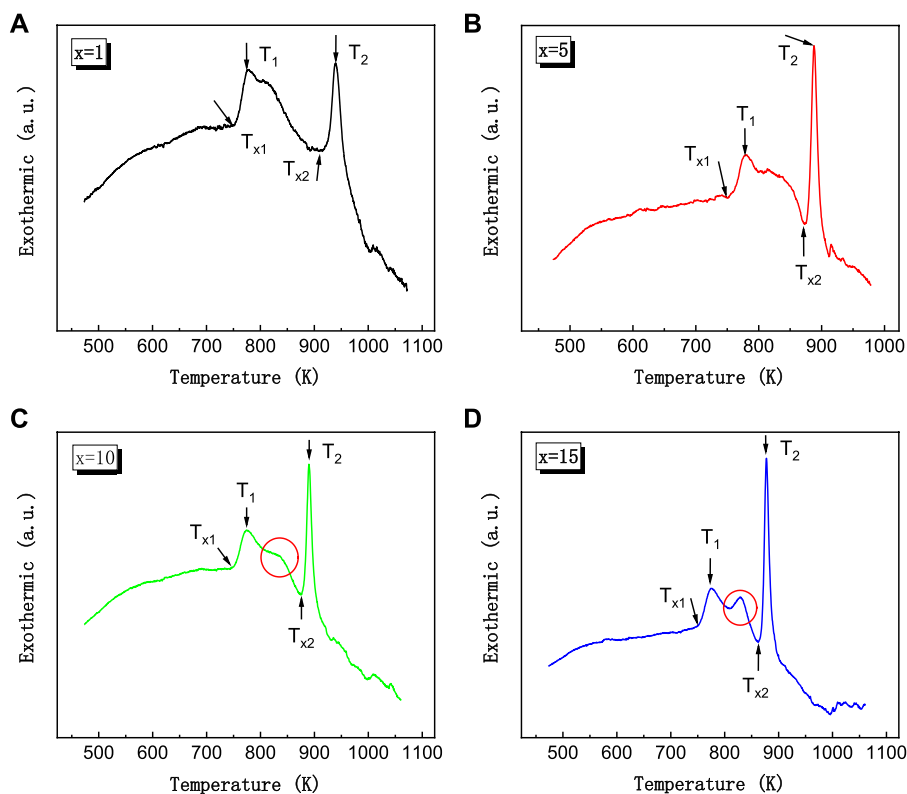


FIGURE 2 | DSC curves of the as-cast $\text{Fe}_{66.8-x}\text{Co}_{10}\text{Ni}_x\text{Cu}_{0.8}\text{Nb}_{2.9}\text{Si}_{11.5}\text{B}_8$ ($x = 1, 5, 10, 15$ at%) ribbons at a heating speed of 10 K/min, **(A)** $x = 1$ alloy, **(B)** $x = 5$ alloy, **(C)** $x = 10$ alloy, **(D)** $x = 15$ alloy.

TABLE 1 | Thermodynamic data of as-cast $\text{Fe}_{66.8-x}\text{Co}_{10}\text{Ni}_x\text{Cu}_{0.8}\text{Nb}_{2.9}\text{Si}_{11.5}\text{B}_8$ ($x = 1, 5, 10, 15$ at%) alloy ribbons.

Alloy	T_{x1} (K)	T_1 (K)	T_{x2} (K)	T_2 (K)	ΔT_x (K)
$x = 1$	757	779	922	940	165
$x = 5$	759	780	878	888	119
$x = 10$	752	774	880	890	128
$x = 15$	750	777	869	877	119

an exothermic-peak-like region between T_{x1} and T_{x2} at about 828 K for the alloys with $x = 10, 15\%$; this region is considered to be an overlap of the two stages of crystallization. It means that the alloys of $\text{Fe}_{56.8}\text{Co}_{10}\text{Ni}_{10}\text{Cu}_{0.8}\text{Nb}_{2.9}\text{Si}_{11.5}\text{B}_8$ and $\text{Fe}_{51.8}\text{Co}_{10}\text{Ni}_{15}\text{Cu}_{0.8}\text{Nb}_{2.9}\text{Si}_{11.5}\text{B}_8$ tend to get into the second crystallization process much more easily. Also, the stability of the first-stage crystallization phase is weaker. This might be the reason for the ΔT_x of the 10% Ni alloy being a little larger than 5% Ni alloy. Values of T_{x1} , T_{x2} , T_1 , T_2 , and ΔT_x of the as-cast $\text{Fe}_{66.8-x}\text{Co}_{10}\text{Ni}_x\text{Cu}_{0.8}\text{Nb}_{2.9}\text{Si}_{11.5}\text{B}_8$ alloys are summarized in **Table 1**.

The cores were annealed at 838 K with transverse magnetic field for 15, 30, and 45 min, respectively. The B-H loops of the cores are shown in **Figure 3**. The hysteresis loops of the annealed alloys show good linearity. With the increment of Ni content, the anisotropic field H_k rises from 200 to 380 A/m. The values of the magnetic anisotropy constant K_u can be obtained from **Eq. 1**.

During the calculation of K_u , J_s was estimated using the values of B_{800} (B_{800} denotes the magnetic induction intensity of alloys under an applied magnetic field of 800 A/m), and the B_{800} values are 1.26, 1.15, 1.11, and 1.04 T for the alloys of Ni = 1%, Ni = 5%, Ni = 10%, and Ni = 15%, respectively. When the Ni content increases to 15%, the alloy exhibits a lower permeability and larger magnetic anisotropy field H_k . However, the coercivity of the alloy is significantly increased, and the linearity of the hysteresis loop gets worse. The coercivity (H_c), remanence (B_r), initial permeability (μ_i), and anisotropy constant (K_u) properties are shown in **Table 2**. With the prolongation of annealing time, the permeability of the alloy gradually decreases. The strength of the magnetic anisotropy field becomes stronger. Moreover, the ability to resist the external magnetic field is enhanced. The H_c and B_r for the $\text{Fe}_{65.8}\text{Co}_{10}\text{Ni}_1\text{Cu}_{0.8}\text{Nb}_{2.9}\text{Si}_{11.5}\text{B}_8$ alloy decrease with the increasing annealing time. The H_c and B_r of $\text{Fe}_{61.8}\text{Co}_{10}\text{Ni}_5\text{Cu}_{0.8}\text{Nb}_{2.9}\text{Si}_{11.5}\text{B}_8$ alloy increase firstly and then get smaller with the increase in heat treatment time. H_c and B_r increase definitely with the heat treatment time when the Ni content is high ($x = 10, 15\%$). When the Ni content reaches 15%, the coercive H_c and the remanence B_r increase greatly. When the heat treatment time increased from 15 to 45 min, H_c and B_r increased from 15.81 A/m and 28 mT to 163.8 A/m and 330 mT, respectively. With the increase in Ni content, the relative initial

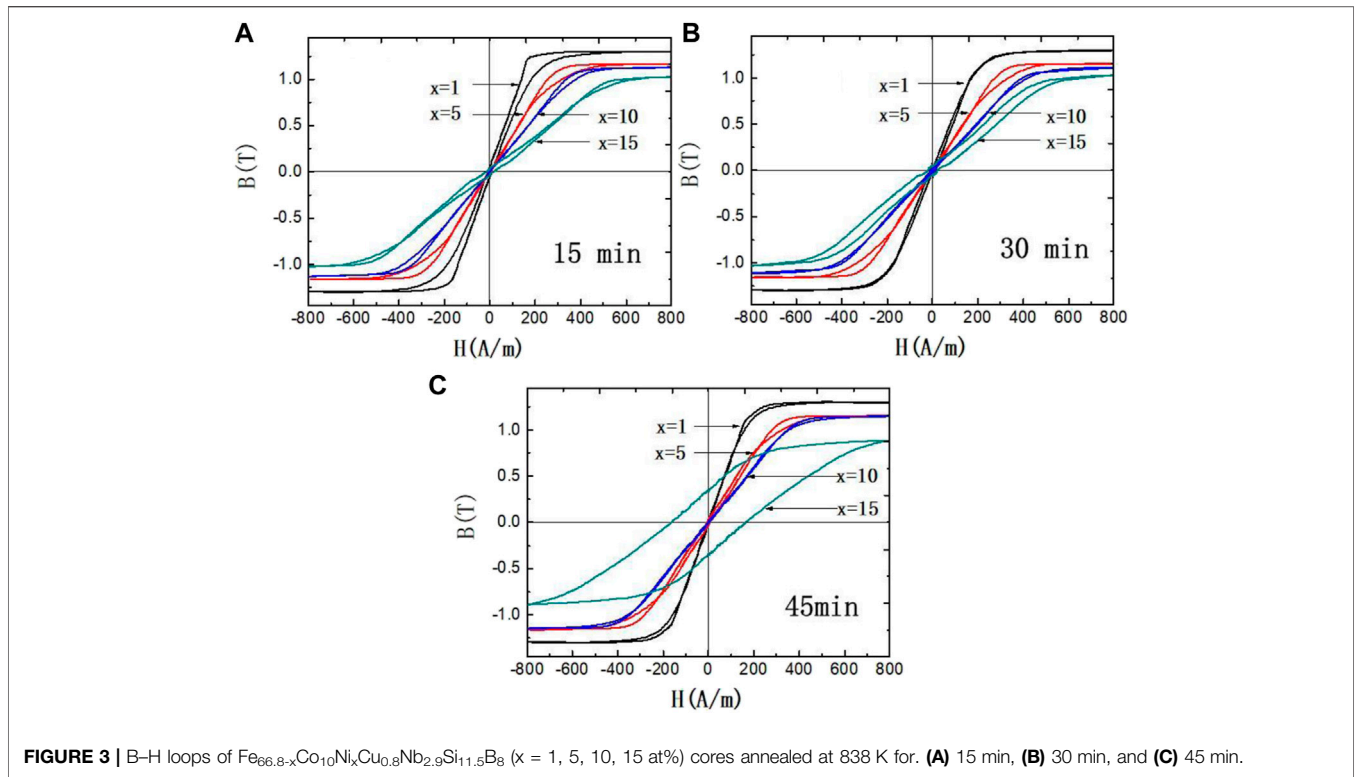


FIGURE 3 | B–H loops of $\text{Fe}_{66.8-x}\text{Co}_{10}\text{Ni}_x\text{Cu}_{0.8}\text{Nb}_{2.9}\text{Si}_{11.5}\text{B}_8$ ($x = 1, 5, 10, 15$ at%) cores annealed at 838 K for. **(A)** 15 min, **(B)** 30 min, and **(C)** 45 min.

TABLE 2 | Magnetic properties of $\text{Fe}_{66.8-x}\text{Co}_{10}\text{Ni}_x\text{Cu}_{0.8}\text{Nb}_{2.9}\text{Si}_{11.5}\text{B}_8$ ($x = 1, 5, 10, 15$ at%) alloy cores.

Alloys	15 min	30 min	45 min
H_c (A/m)			
$x = 1$	7.93	0.54	0.40
$x = 5$	3.21	0.41	0.65
$x = 10$	0.21	0.61	0.84
$x = 15$	15.81	19.41	163.8
B_r (mT)			
$x = 1$	55.71	30.55	23.92
$x = 5$	31.91	23.41	23.88
$x = 10$	2.35	2.35	7.44
$x = 15$	27.6	63.2	329.5
μ_i			
$x = 1$	5,300	5,100	5,400
$x = 5$	3,050	2,940	2,660
$x = 10$	2,290	2,000	2,230
$x = 15$	1,310	810	580
K_u (J/m^3)			
$x = 1$	108	126	129
$x = 5$	163	170	174
$x = 10$	204	225	200
$x = 15$	232	257	355

permeability μ_i decreases and the magnetic anisotropy K_u is enhanced.

The XRD patterns of $\text{Fe}_{66.8-x}\text{Co}_{10}\text{Ni}_x\text{Cu}_{0.8}\text{Nb}_{2.9}\text{Si}_{11.5}\text{B}_8$ ($x = 1, 5, 10, 15$ at%) alloy ribbons which annealed at 838 K for 30 min are shown in **Figure 4**. The grain size of the crystalline phase was estimated using the Scherrer formula as follows (Scherrer, 1918),

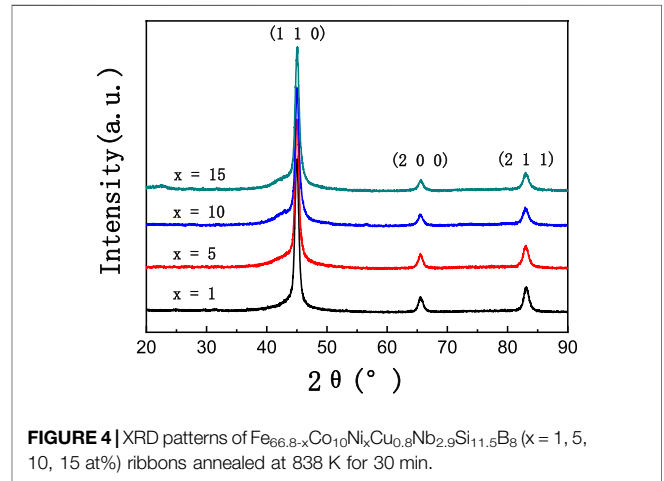
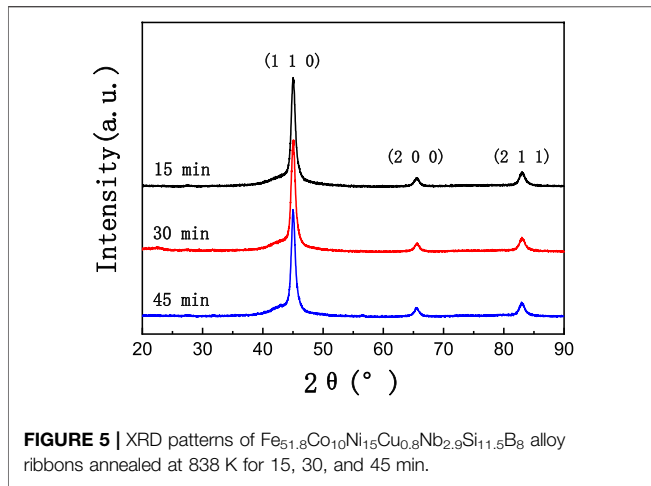


FIGURE 4 | XRD patterns of $\text{Fe}_{66.8-x}\text{Co}_{10}\text{Ni}_x\text{Cu}_{0.8}\text{Nb}_{2.9}\text{Si}_{11.5}\text{B}_8$ ($x = 1, 5, 10, 15$ at%) ribbons annealed at 838 K for 30 min.

$$D = \frac{K\lambda}{\beta \cos \theta} \tag{2}$$

where D is the grain size, K is the Scherrer constant (~ 0.89), λ is the wavelength of the X-ray, β is the full width at half maximum (FWHM) of the diffraction peak, and θ is the Bragg angle. The crystallized volume fraction phase can be estimated by using the following equation (Langford, 1978; Verdon et al., 1998; Zhang et al., 1998; Cerqueira et al., 2000; Aronin et al., 2010):

$$V_{cr} = \frac{I_{cr}}{I_{cr} + I_{am}} \tag{3}$$



where V_{cr} is the crystallized volume fraction, and I_{cr} and I_{am} denote the integrated peak intensities of the crystalline and amorphous phases, respectively.

According to the XRD patterns, the first crystallization process of the $\text{Fe}_{66.8-x}\text{Co}_{10}\text{Ni}_x\text{Cu}_{0.8}\text{Nb}_{2.9}\text{Si}_{11.5}\text{B}_8$ ($x = 1, 5, 10, 15$ at%) samples is characterized by the precipitation of α -Fe and some α - Fe_3Si crystalline phase. Additionally, Co and Ni atoms partially substitute the crystallographic positions of Fe atoms in the precipitated crystalline phases, leading to the formation of α -(Fe, Ni), α -(Fe, Co), and α -(Fe, Co, Ni) $_3$ Si phases with a bcc structure. Although there is an overlap area between the two crystallization temperatures at about 833 K, there is no other phase but bcc. Maybe the content of the possibly existing phase is very small that we cannot find it through XRD results. The crystallized volume fraction is about 25%, and the grain size is about 11–15 nm. The main diffraction peak positions (2θ) in XRD patterns for the $\text{Fe}_{66.8-x}\text{Co}_{10}\text{Ni}_x\text{Cu}_{0.8}\text{Nb}_{2.9}\text{Si}_{11.5}\text{B}_8$ ($x = 1, 5, 10, 15$ at%) alloys are 44.92°, 44.94°, 45.03°, and 45.00°, respectively. The main diffraction peak positions (2θ) and lattice constants for the α -Fe, α - Fe_3Si , α -(Fe,Ni), and α -(Fe, Co) phases are 44.673°, 45.186°, 44.645°, 44.827°, and 2.8664, 2.841, 2.8681, and 2.8570 Å, respectively. As the Ni content increases in the $\text{Fe}_{66.8-x}\text{Co}_{10}\text{Ni}_x\text{Cu}_{0.8}\text{Nb}_{2.9}\text{Si}_{11.5}\text{B}_8$ alloys, the solubility of Ni and Si in the crystalline phases increases during the crystallization process, causing severer lattice distortion. During the amorphous-to-crystalline transformation process, a proportion of energy is consumed to compensate for the elevated lattice distortion energy, so the crystallization enthalpy of the first crystallization stage declines.

Based on the random anisotropy model (Herzer, 1989), the magnetic anisotropy is mainly determined by the grain size (D) and the crystallized volume fraction (χ). Specifically, magnetic anisotropy is positively correlated with grain size. The corresponding quantitative correlation can be expressed as below:

$$\langle K \rangle = |K_1| \cdot \chi^2 (D/L_0)^6 \quad (4)$$

where $\langle K \rangle$ is the effective anisotropy constant, K_1 is the magnetic anisotropy constant, and L_0 denotes the exchange length. The

coercivity H_c and initial permeability μ_i can be expressed as the following equations:

$$H_c = P_c \frac{\langle K \rangle}{J_s} \quad (5)$$

$$\mu_i = P_c \frac{J_s^2}{\mu_0 \langle K \rangle} \quad (6)$$

where P_c is a dimensionless constant, J_s is the saturation magnetic polarization of the material, and μ_0 is the vacuum permeability. The rise in H_c of soft magnetic alloys is mainly due to the increment in grain size.

The XRD patterns of the $x = 15$ alloy ribbons annealed at 838 K for 15, 30, and 45 min are shown in Figure 5. The crystallized volume fractions of the samples shown in Figure 5 are all about 25%, while the corresponding grain size is 11–15 nm. The crystalline phases are consistent with the previous analysis. So, the reason for the sharp increase in H_c of the alloy annealed for 45 min is not caused by the increase in grain size. The diffraction peak positions and the lattice constant of the ribbons which were annealed for 15, 30, and 45 min are 44.980°, 45.000°, and 44.960° and 2.8478, 2.8466, and 2.8490 Å, respectively. Therefore, the drastic increase in coercivity is not caused by the difference in the degree of lattice distortion, either.

The theory proposed by Luborsky (Luborsky et al., 1976) suggests that the origin of the induced anisotropy K_u in the amorphous alloys is the atomic pairing orientation, which is the same as that of the crystalline material. Since the crystallization process is a thermal activation process, the coupling orientation of (Fe, Ni) atoms would be enhanced as the annealing time increases. The magnetic anisotropy was enhanced then. The rise in H_c could be ascribed to the enhanced magnetic anisotropy or the change in magnetic domain structure after the enhancement magnetic anisotropy.

The permeability-vs.-frequency curves of $\text{Fe}_{66.8-x}\text{Co}_{10}\text{Ni}_x\text{Cu}_{0.8}\text{Nb}_{2.9}\text{Si}_{11.5}\text{B}_8$ ($x = 1, 5, 10, 15$ at%) alloy cores which were annealed at 838 K for 30 min are shown in Figure 6. With the increase in Ni content, the initial permeability of the alloy becomes lower and the magnetic anisotropy is enhanced. The decay of relative initial magnetic

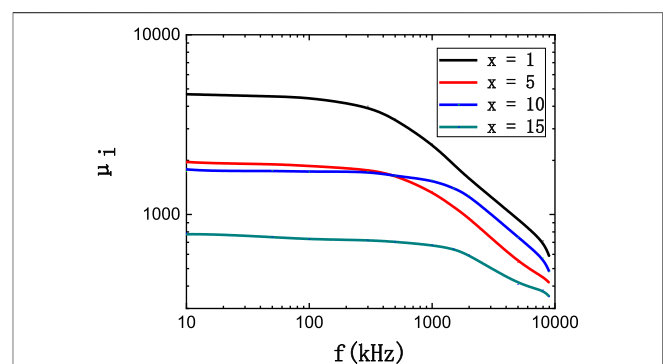


FIGURE 6 | The permeability–frequency curves of $\text{Fe}_{66.8-x}\text{Co}_{10}\text{Ni}_x\text{Cu}_{0.8}\text{Nb}_{2.9}\text{Si}_{11.5}\text{B}_8$ ($x = 1, 5, 10, 15$ at%) alloy cores.

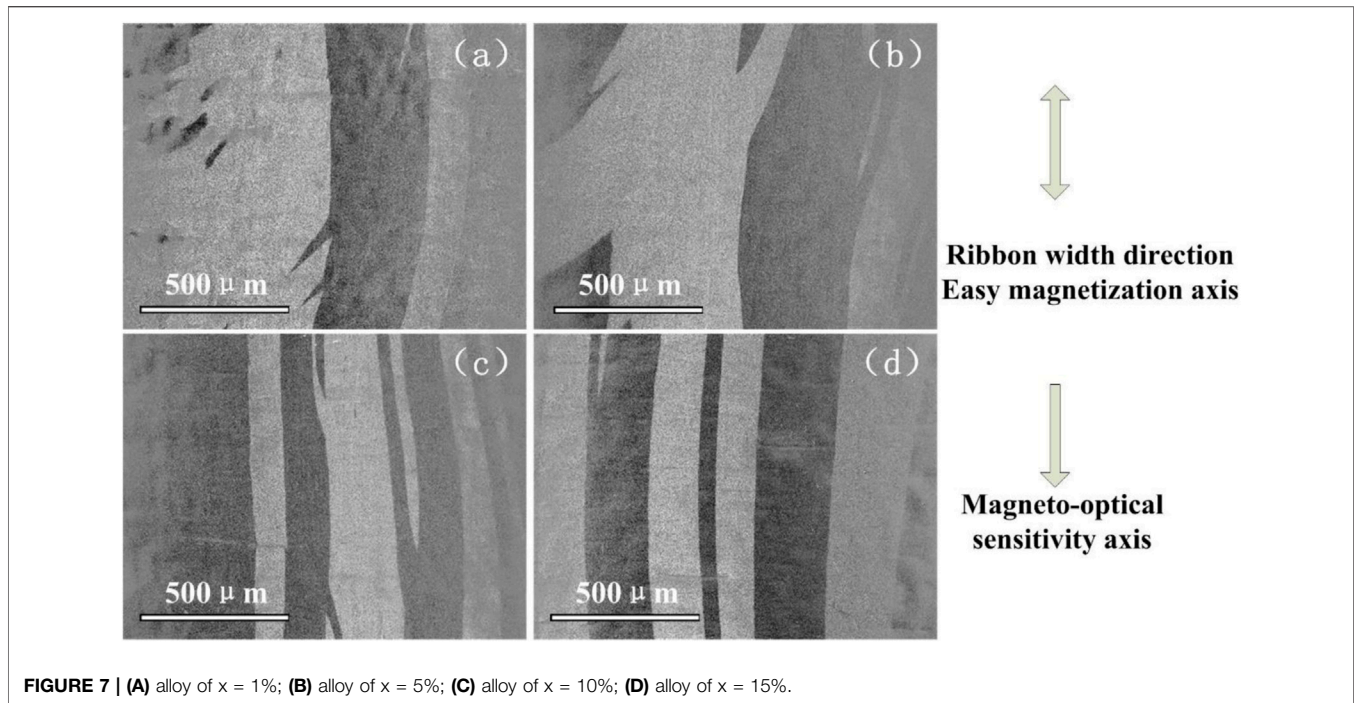


FIGURE 7 | (A) alloy of $x = 1\%$; **(B)** alloy of $x = 5\%$; **(C)** alloy of $x = 10\%$; **(D)** alloy of $x = 15\%$.

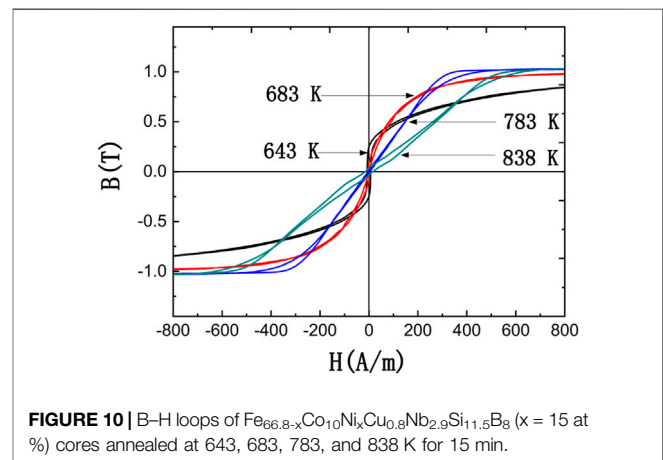
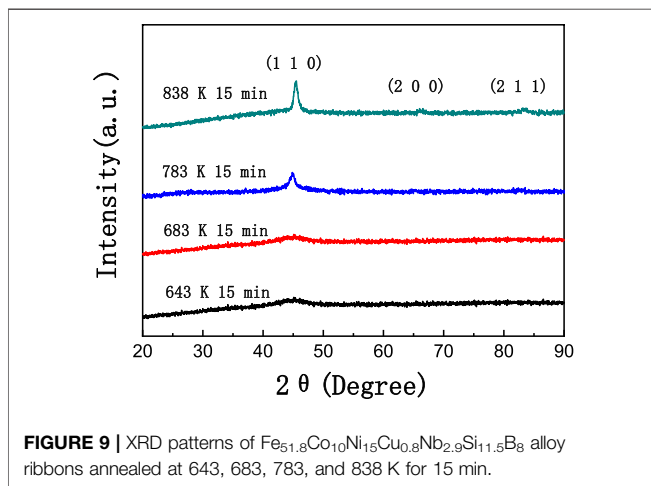
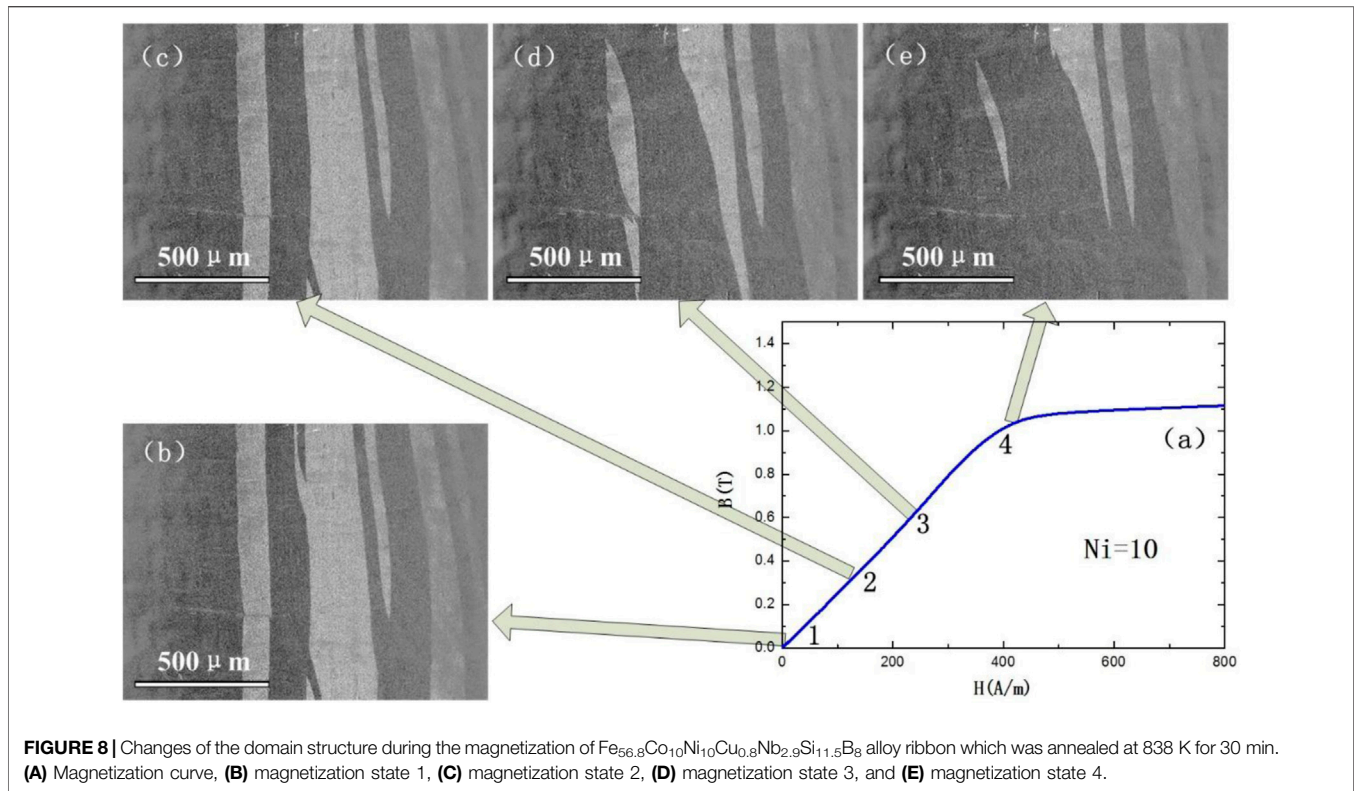
permeability became slower with the increase in frequency. The permeability of the alloy with a Ni content of 10% is about 2,000, and the magnetic field induced K_u is about 225 J/m^3 . The permeability attenuation of these alloys was 47.8%, 35.2%, 19.2%, and 10.2% from 10 to 1,000 kHz for the alloy with Ni content of 1%, 5%, 10%, and 15%, respectively. These results agree with the previous work by Ohnuma in Ref. (Herzer, 1994b) that, with the increase of K_u , the alloy exhibits more excellent permeability-vs.-frequency characteristics in the high-frequency band.

The domain structures of $\text{Fe}_{66.8-x}\text{Co}_{10}\text{Ni}_x\text{Cu}_{0.8}\text{Nb}_{2.9}\text{Si}_{11.5}\text{B}_8$ ($x = 1, 5, 10, 15 \text{ at}\%$) alloy ribbons annealed at 838 K for 30 min are shown in **Figure 7**. The double arrow line in **Figure 7** denotes the width direction of the ribbon, which is parallel to the direction of the transverse magnetic field during annealing. The single arrow line is parallel to the orientation of the polarized light in the magneto-optical Kerr microscope. The light-colored magnetic domains are oriented in the same direction as the polarized light, while the dark magnetic domains are in the opposite direction of the polarized light. It can be concluded from the figure that the size of the magnetic domain decreases when the magnetic anisotropy intensity becomes stronger with the increase in the Ni content. The parallelism between the magnetic domain and the direction of the applied magnetic field becomes stronger. The local magnetic domain structure becomes more uniformly distributed. From the perspective of technical magnetization, the magnetic domain structure inside the material because the sum of the different energies tends to be minimized. Moreover, the corresponding energies can be categorized as the exchange energy, the magneto-elastic energy, the magneto-crystalline anisotropy, the demagnetizing field energy, and the applied magnetic field energy. This result agrees with the work by

Herzer (Herzer et al., 2011) that combines the domain structure and creep-induced K_u .

The changing process of $x = 10\%$ alloy's domain structure during the whole magnetization process is shown in **Figure 8**. The direction distribution and test method of the magnetic domain structure photo are the same as those in **Figure 7**. The magnetic domain structure in each magnetized state is shown in the photograph indicated by the arrow in the figure. The magnetic domain of the alloy ribbon is fine 90° structure, and the whole magnetization process is basically a reversible movement of the domain walls. According to the magnetization theory of soft magnetic materials, the magnetization process can be separated into five steps (Tahara and Sugeno, 1973; Iványi, 1997). First is the initial magnetization (μ_i), or the so-called linear magnetization region, where B varies linearly with H . Second is the Rayleigh region, where the magnetization process is no longer linear. Third is the maximum permeability region, where B increases sharply with H . Fourth is the near saturation region. Fifth is the paramagnetic region. In the magnetization process of $\text{Fe}_{61.8}\text{Co}_{10}\text{Ni}_5\text{Cu}_{0.8}\text{Nb}_{2.9}\text{Si}_{11.5}\text{B}_8$ and $\text{Fe}_{56.8}\text{Co}_{10}\text{Ni}_{10}\text{Cu}_{0.8}\text{Nb}_{2.9}\text{Si}_{11.5}\text{B}_8$ alloy ribbons, the first region is very big, and the second to fourth regions become very small. So, the magnetization process is kept linear until saturation.

For the $\text{Fe}_{51.8}\text{Co}_{10}\text{Ni}_{15}\text{Cu}_{0.8}\text{Nb}_{2.9}\text{Si}_{11.5}\text{B}_8$ alloy ribbon, more Ni elements may be entrapped in the $\alpha\text{-(Fe)}$ and $\alpha\text{-(Fe)}_3\text{Si}$ crystallization phases to replace the Fe atom position during the heat treatment. It will result in a more serious lattice distortion, so the energy of the alloy system increases. In addition, the addition of the Ni element increases the number of magnetic interaction (Fe, Ni) atom pairs in the alloy and enhances the magnetic anisotropy. In order to reduce the energy



of the alloy, the magnetic field size of the soft magnetic alloy becomes smaller. This makes the B-H loop of the alloy with strong magnetic anisotropy show poor linearity, and its coercivity and remanence are larger.

Since the soft magnetic properties of the $\text{Fe}_{51.8}\text{Co}_{10}\text{Ni}_{15}\text{Cu}_{0.8}\text{Nb}_{2.9}\text{Si}_{11.5}\text{B}_8$ alloy are very poor, some further heat treatment was applied to the cores. The deterioration of the coercivity property was originated in the distortion of the lattice. It was assumed that the distortion could be reduced by the decrease in the crystallization degree. We chose a temperature that is higher than the crystallization temperature

and definitely lower than the overlap region. Moreover, some other temperatures that are lower than the crystallization temperature were set. The heat treatment temperatures were 783, 683, and 643 K then, and the heat treatment time was 15 min. The heat treatment was finished when the furnace was cooled to 473 K, and the transverse magnetic field of 400 Oe was applied. The XRD patterns of the $\text{Fe}_{51.8}\text{Co}_{10}\text{Ni}_{15}\text{Cu}_{0.8}\text{Nb}_{2.9}\text{Si}_{11.5}\text{B}_8$ alloy ribbons after heat treatment are shown in **Figure 9**. The crystallization temperature of the alloy is 750 K, and the first crystallization peak temperature is 777 K. Some α -Fe-crystallized phases were formed after the heat treatment at 783 K for 15 min. After

TABLE 3 | Properties of the different temperature-annealed Fe_{51.8}Co₁₀Ni₁₅Cu_{0.8}Nb_{2.9}Si_{11.5}B₈ alloy.

Properties	838 K	643 K	683 K	783 K
H _c (A/m)	15.81	7.29	4.11	3.63
B _r (mT)	27.6	250.9	80.7	12.2
μ _i	1,310	13,780	8,090	2,560
K _u (J/m ³)	232	—	—	180

calculation, the crystallization ratio is less than 5%. Both 683 and 643 K were subjected to stress relief annealing, and the alloy ribbons possess a typical amorphous structure after heat treatment.

The B–H loops of these Fe_{51.8}Co₁₀Ni₁₅Cu_{0.8}Nb_{2.9}Si_{11.5}B₈ alloy are shown in **Figure 10**. The μ_i, H_c, and B_r properties are listed in **Table 3**. With the increase in heat treatment temperature, the linearity of the B–H loop gradually increased; meanwhile, the remanence and coercivity decreased. When the heat treatment temperature rises from 643 to 783, the coercivity of the alloy decreases from 7.29 to 3.63 A/m, and the remanence is reduced from 250.9 to 12.2 mT. However, when the heat treatment temperature increased to 838 K, the coercivity of the alloy increased to 15.81 A/m, and remanence increased to 27.6 mT. It seems that the trace crystallization is beneficial to obtain excellent soft magnetic properties for the Fe-based alloy with high content of Ni. To obtain better soft magnetic properties, it can be summarized as the following: the higher the Ni content, the lower the heat treatment temperature required.

SUMMARY

The crystallization behavior, microstructure, soft magnetic properties, and domain structure for Fe_{66.8-x}Co₁₀Ni_xCu_{0.8}Nb_{2.9}Si_{11.5}B₈ alloys with the Ni content ranging from x = 1 to x = 15 have been systemically studied, and results are summarized as follows:

1. The increment of the Ni content results in the decline of the crystallization temperature of the secondary crystallization phase and decreases the thermal stability of the α-Fe phase.

REFERENCES

- Agudo, P., and Vázquez, M. (2005). Influence of Ni on the Structural and Magnetic Properties of Ni_xFe_{73.5-x}Si_{13.5}B₉Nb₃Cu₁ (0 ≤ x ≤ 25) Alloys. *J. Appl. Phys.* 97, 023901. doi:10.1063/1.1825633
- Aronin, A., Abrosimova, G., Matveev, D., and Rybchenko, O. (2010). Structure and Properties of Nanocrystalline. *Rev. Adv. Mater. Sci.* 25, 52–57.
- Cerqueira, M. F., Ferreira, J. A., and Adriaenssens, G. J. (2000). Structural Studies and Influence of the Structure on the Electrical and Optical Properties of Microcrystalline Silicon Thin Films Produced by RF Sputtering. *Thin Solid Films* 370, 128–136. doi:10.1016/S0040-6090(00)00950-0
- Chen, F. G., Wang, Y. G., Miao, X. F., Hong, H., and Bi, K. (2013). Nanocrystalline Fe₈₃P₁₆Cu₁ Soft Magnetic alloy Produced by Crystallization of its Amorphous Precursor. *J. Alloys Compd.* 549, 26–29. doi:10.1016/j.jallcom.2012.09.072
- Fujimori, H., Morita, H., Obi, Y., and Ohta, S. (1977). "On the Magnetically Induced Anisotropy in Amorphous Ferromagnetic Alloys," in *Amorphous*

The temperature interval between the two crystallization processes is drastically reduced from 165 to 119 K when the Ni content increases from x = 1 to x = 15.

2. With the increase in Ni content, the magnetic anisotropy of the alloy is enhanced. However, when the Ni content is ≥15%, the coercivity and remanence properties of the alloy deteriorate sharply. The low coercivity and remanence properties can be obtained by reducing the heat treatment temperature, and the B–H loop linearity of the alloy is improved.
3. A large magnetic field-induced K_u of 225 J/m³ can be obtained through optimized annealing, and the Fe_{56.8}Co₁₀Ni₁₀Cu_{0.8}Nb_{2.9}Si_{11.5}B₈ nanocrystalline alloy exhibits a linear B–H loop and its initial permeability μ_i is as low as 2,000. It makes the alloy a promising material in the field of common mode chokes or current transformers, where the ability to resist the direct current is necessary.

DATA AVAILABILITY STATEMENT

The original contributions presented in the study are included in the article/Supplementary Material; further inquiries can be directed to the corresponding author.

AUTHOR CONTRIBUTIONS

ZL, the first person to complete the thesis work. KY, provided ideas for this work and finished the thesis together. TL, provided materials to finish the experimental works. XL, participated the testing work. SW, provided suggestions for the completion of the thesis.

FUNDING

This work was supported by the National Key Basic Research and Development Program (Grant No. 2016YFB0300502), National Natural Science Foundation of China (11875270), and Youth Innovation Promotion Association CAS (2018015).

Magnetism II. Editors R. A. Levy and R. Hasegawa (New York: Plenum), 393–402. doi:10.1007/978-1-4613-4178-9_37

Hasegawa, R. (2006). Advances in Amorphous and Nanocrystalline Magnetic Materials. *J. Magn. Magn. Mater.* 304, 187–191. doi:10.1016/j.jmmm.2006.02.119

Hasegawa, R. (2004). Applications of Amorphous Magnetic Alloys. *Mater. Sci. Eng. A*. 375, 90–97. doi:10.1016/j.msea.2003.10.258

Herzer, G., Budinsky, V., and Polak, C. (2011). Magnetic Properties of FeCuNbSiB Nanocrystallized by Flash Annealing under High Tensile Stress. *Phys. Status Solidi B* 248, 2382–2388. doi:10.1002/pssb.201147088

Herzer, G. (1994). Creep Induced Magnetic Anisotropy in Nanocrystalline Fe-Cu-Nb-Si-B Alloys. *IEEE Trans. Magn.* 30, 4800–4802. doi:10.1109/20.334226

Herzer, G. (1989). Grain Structure and Magnetism of Nanocrystalline Ferromagnets. *IEEE Trans. Magn.* 25, 3327–3329. doi:10.1109/20.42292

Herzer, G. (1994). Magnetic Field Induced Anisotropy in Nanocrystalline Fe Cu Nb Si B Alloys. *Mater. Sci. Eng. A* 181–182, 876–879. doi:10.1016/0921-5093(94)90760-9

- Herzer, G. (2013). Modern Soft Magnets: Amorphous and Nanocrystalline Materials. *Acta Materialia* 61, 718–734. doi:10.1016/j.actamat.2012.10.040
- Herzer, G., Vazquez, M., Knobel, M., Zhukov, A., Reininger, T., Davies, H. A., et al. (2005). Round Table Discussion: Present and Future Applications of Nanocrystalline Magnetic Materials. *J. Magnetism Magn. Mater.* 294, 252–266. doi:10.1016/j.jmmm.2005.03.042
- Iványi, A. (1997). *Hysteresis Models in Electromagnetic Computation*. Budapest, Hungary: University of Pécs, Book, Akadémiai Kiadó.
- Kubota, T., Makino, A., and Inoue, A. (2011). Low Core Loss of Fe₈₅Si₂B₈P₄Cu₁ Nanocrystalline Alloys with High Bs and B800. *J. Alloys Compd.* 509, S416–S419. doi:10.1016/j.jallcom.2010.11.012
- Langford, J. I. (1978). A Rapid Method for Analysing the Breadths of Diffraction and Spectral Lines Using the Voigt Function. *J. Appl. Cryst.* 11, 10–14. doi:10.1107/s0021889878012601
- Li, J.-F., Liu, X., Zhao, S.-F., Ding, H.-Y., and Yao, K.-F. (2015). Fe-based Bulk Amorphous Alloys with Iron Contents as High as 82at%. *J. Magnetism Magn. Mater.* 386, 107–110. doi:10.1016/j.jmmm.2015.03.070
- Li, Z., Wang, A., Chang, C., Wang, Y., Dong, B., and Zhou, S. (2014). Synthesis of FeSiBPNbCu Nanocrystalline Soft-Magnetic Alloys with High Saturation Magnetization. *J. Alloys Compd.* 611, 197–201. doi:10.1016/j.jallcom.2014.04.223
- Luborsky, F. E., Becker, J. J., Lander, G. H., and Rhyne, J. J. (1976). "Kinetics of reorientation of magnetically induced anisotropy in amorphous Ni₄₀Fe₄₀P₁₄B₆," in AIP Conference Proceedings 29, 209–210. doi:10.1063/1.30588
- Makino, A., He Men, H., Kubota, T., Yubuta, K., and Inoue, A. (2009). New Excellent Soft Magnetic FeSiBPCu Nanocrystallized Alloys with High B_{50} of 1.9 T from Nanohetero-Amorphous Phase. *IEEE Trans. Magn.* 45, 4302–4305. doi:10.1109/tmag.2009.2023862
- Makino, A., Inoue, A., and Masumoto, T. (1995). Soft Magnetic Properties of Nanocrystalline Fe M B(M Zr, Hf, Nb) Alloys with High Magnetization. *Nanostructured Mater.* 6, 985–988. doi:10.1016/0965-9773(95)00226-x
- Ohnuma, M., Ping, D. H., Abe, T., Onodera, H., Hono, K., and Yoshizawa, Y. (2003). Optimization of the Microstructure and Properties of Co-substituted Fe-Si-B-Nb-Cu Nanocrystalline Soft Magnetic Alloys. *J. Appl. Phys.* 93, 9186–9194. doi:10.1063/1.1569396
- Ohta, M., and Yoshizawa, Y. (2007). New High-BsFe-Based Nanocrystalline Soft Magnetic Alloys. *Jpn. J. Appl. Phys.* 46, L477–L479. doi:10.1143/jjap.46.L477
- Petzold, J. (2002). Advantages of Softmagnetic Nanocrystalline Materials for Modern Electronic Applications. *J. Magnetism Magn. Mater.* 242–245, 84–89. doi:10.1016/s0304-8853(01)01206-9
- Scherrer, P. (1918). Bestimmung der Größe und der inneren Struktur von Kolloidteilchen mittels Röntgenstrahlen. *Nachr. Ges. Wiss. Göttingen, Math.-Phys. Kl.* 26, 98.
- Shi, L., Hu, X., Li, Y., Yuan, G., and Yao, K. (2021). The Complementary Effects of Fe and Metalloids on the Saturation Magnetization of Fe-Based Amorphous Alloys. *Intermetallics* 131, 107116. doi:10.1016/j.intermet.2021.107116
- Shi, L., and Yao, K. (2020). Composition Design for Fe-Based Soft Magnetic Amorphous and Nanocrystalline Alloys with High Fe Content. *Mater. Des.* 189, 108511. doi:10.1016/j.matdes.2020.108511
- Tahara, Y., and Sugeno, T. (1973). A Theory of Magnetic After-Effect for the Irreversible Magnetization Process in Rayleigh Region. *Phys. Stat. Sol. (B)* 55, 385–398. doi:10.1002/pssb.2220550140
- Urata, A., Matsumoto, H., Yoshida, S., and Makino, A. (2011). Fe-B-P-Cu Nanocrystalline Soft Magnetic Alloys with High Bs. *J. Alloys Compd.* 509, S431–S433. doi:10.1016/j.jallcom.2010.12.104
- Verdon, C., Karimi, A., and Martin, J.-L. (1998). A Study of High Velocity Oxy-Fuel Thermally Sprayed Tungsten Carbide Based Coatings. Part I: Microstructures. *Mater. Sci. Eng. A* 246, 11–24. doi:10.1016/s0921-5093(97)00759-4
- Yoshizawa, Y., Fujii, S., Ping, D. H., Ohnuma, M., and Hono, K. (2003). Magnetic Properties of Nanocrystalline FeMCuNbSiB Alloys (M: Co, Ni). *Scripta Materialia* 48, 863–868. doi:10.1016/s1359-6462(02)00611-5
- Yoshizawa, Y., Oguma, S., and Yamauchi, K. (1988). New Fe-based Soft Magnetic Alloys Composed of Ultrafine Grain Structure. *J. Appl. Phys.* 64, 6044–6046. doi:10.1063/1.342149
- Yoshizawa, Y., Yamauchi, K., Yamane, T., and Sugihara, H. (1988). Common Mode Choke Cores Using the New Fe-based Alloys Composed of Ultrafine Grain Structure. *J. Appl. Phys.* 64, 6047–6049. doi:10.1063/1.342150
- Zhang, X. Y., Zhang, F. X., Zhang, J. W., Yu, W., Zhang, M., Zhao, J. H., et al. (1998). Influence of Pressures on the Crystallization Process of an Amorphous Fe_{73.5}Cu₁Nb₃Si_{13.5}B₉ alloy. *J. Appl. Phys.* 84, 1918–1923. doi:10.1063/1.368319

Conflict of Interest: TL was employed by the company China Iron and Steel Research Institute Group, Advanced Technology and Materials Co., Ltd.

The remaining authors declare that the research was conducted in the absence of any commercial or financial relationships that could be construed as a potential conflict of interest.

Publisher's Note: All claims expressed in this article are solely those of the authors and do not necessarily represent those of their affiliated organizations, or those of the publisher, the editors, and the reviewers. Any product that may be evaluated in this article, or claim that may be made by its manufacturer, is not guaranteed or endorsed by the publisher.

Copyright © 2022 Li, Yao, Liu, Li and Wang. This is an open-access article distributed under the terms of the Creative Commons Attribution License (CC BY). The use, distribution or reproduction in other forums is permitted, provided the original author(s) and the copyright owner(s) are credited and that the original publication in this journal is cited, in accordance with accepted academic practice. No use, distribution or reproduction is permitted which does not comply with these terms.